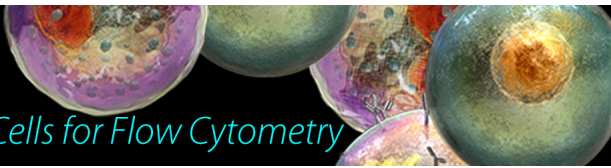


Veri-Cells™

Verified Lyophilized Control Cells for Flow Cytometry



This information is current as of July 19, 2018.

ERK2-Dependent Activation of c-Jun Is Required for Nontypeable *Haemophilus influenzae*-Induced CXCL2 Upregulation in Inner Ear Fibrocytes

Sejo Oh, Jeong-Im Woo, David J. Lim and Sung K. Moon

J Immunol 2012; 188:3496-3505; Prepublished online 29 February 2012;
doi: 10.4049/jimmunol.1103182
<http://www.jimmunol.org/content/188/7/3496>

Supplementary Material <http://www.jimmunol.org/content/suppl/2012/02/29/jimmunol.1103182.DC1>

References This article **cites 91 articles**, 24 of which you can access for free at:
<http://www.jimmunol.org/content/188/7/3496.full#ref-list-1>

Why *The JI*? Submit online.

- **Rapid Reviews! 30 days*** from submission to initial decision
- **No Triage!** Every submission reviewed by practicing scientists
- **Fast Publication!** 4 weeks from acceptance to publication

**average*

Subscription Information about subscribing to *The Journal of Immunology* is online at:
<http://jimmunol.org/subscription>

Permissions Submit copyright permission requests at:
<http://www.aai.org/About/Publications/JI/copyright.html>

Email Alerts Receive free email-alerts when new articles cite this article. Sign up at:
<http://jimmunol.org/alerts>

The Journal of Immunology is published twice each month by
The American Association of Immunologists, Inc.,
1451 Rockville Pike, Suite 650, Rockville, MD 20852
Copyright © 2012 by The American Association of
Immunologists, Inc. All rights reserved.
Print ISSN: 0022-1767 Online ISSN: 1550-6606.



ERK2-Dependent Activation of c-Jun Is Required for Nontypeable *Haemophilus influenzae*-Induced CXCL2 Upregulation in Inner Ear Fibrocytes

Sejo Oh,^{*,1} Jeong-Im Woo,^{*,1} David J. Lim,^{*,†} and Sung K. Moon^{*}

The inner ear, composed of the cochlea and the vestibule, is a specialized sensory organ for hearing and balance. Although the inner ear has been known as an immune-privileged organ, there is emerging evidence indicating an active immune reaction of the inner ear. Inner ear inflammation can be induced by the entry of proinflammatory molecules derived from middle ear infection. Because middle ear infection is highly prevalent in children, middle ear infection-induced inner ear inflammation can impact the normal development of language and motor coordination. Previously, we have demonstrated that the inner ear fibrocytes (spiral ligament fibrocytes) are able to recognize nontypeable *Haemophilus influenzae*, a major pathogen of middle ear infection, and upregulate a monocyte-attracting chemokine through TLR2-dependent NF- κ B activation. In this study, we aimed to determine the molecular mechanism involved in nontypeable *H. influenzae*-induced cochlear infiltration of polymorphonuclear cells. The rat spiral ligament fibrocytes were found to release CXCL2 in response to nontypeable *H. influenzae* via activation of c-Jun, leading to the recruitment of polymorphonuclear cells to the cochlea. We also demonstrate that MEK1/ERK2 signaling pathway is required for nontypeable *H. influenzae*-induced CXCL2 upregulation in the rat spiral ligament fibrocytes. Two AP-1 motifs in the 5'-flanking region of CXCL2 appeared to function as a nontypeable *H. influenzae*-responsive element, and the proximal AP-1 motif was found to have a higher binding affinity to nontypeable *H. influenzae*-activated c-Jun than that of the distal one. Our results will enable us better to understand the molecular pathogenesis of middle ear infection-induced inner ear inflammation. *The Journal of Immunology*, 2012, 188: 3496–3505.

The inner ear, a sensory organ for hearing and balance, is composed of various types of cells such as sensory hair cells and nonsensory supporting cells (1, 2). Like the brain and the eyes, the inner ear has been known as an immune-privileged organ associated with a blood–labyrinthine barrier (3, 4). However, there is emerging evidence that the inner ear is not an immunologically inactive organ. Tissue-resident macrophages were found to constitutively exist in the spiral ligament and spiral ganglion of the cochlea (5). The external sulcus cells of the cochlea also appeared to express a pathogen recognition receptor, TLR4 (6). Moreover, the fibrocytes in the spiral ligament are known to respond to a systemic challenge of endotoxin (7).

The spiral ligament fibrocytes (SLFs), the most abundant inner ear cell type, express a variety of ion channels such as Na⁺/K⁺-ATPase and connexin 26 (8, 9) serving as a part of the potassium recycle pathway required for normal hearing (10, 11). According

to the ion channels expressed, the SLFs are divided into several types (12). Notably, one type of SLF activates NF- κ B in response to noise exposure, whereas another type mainly responds to a systemic challenge of LPS (7). The SLFs can release inflammatory mediators in response to proinflammatory cytokines (13) and otitis media (OM) pathogens such as *Streptococcus pneumoniae* and nontypeable *Haemophilus influenzae* (14).

OM is one of the most common pediatric infectious diseases and is attributed to generate >20 million physician visits per year in the United States (15). As a complication, OM can lead to inner ear inflammation, that is, serous and purulent labyrinthitis (16), resulting in sensorineural hearing loss (SNHL) (17) and vertigo (18). OM-induced inner ear inflammation in children is clinically important because it can result in a delay in the development of language (19) and motor coordination (20). However, it is not easy to detect OM-induced SNHL with a conventional hearing test because it is frequently transient and limited in the ultrahigh frequency (21, 22).

OM-induced inner ear inflammation is evoked by the entry of bacterial molecules of OM pathogens into the inner ear through the round window membrane (23). It has been demonstrated that pneumococcal OM results in hair cell loss (24) and pathologic changes in the cochlear lateral wall (25, 26) in animal studies. However, the molecular mechanism involved in OM-induced inner ear inflammation remains unclear. Recently, we have shown that the SLFs induce MCP-1/CCL2 in response to nontypeable *H. influenzae* through TLR2-dependent NF- κ B activation (27), and SLF-derived MCP-1/CCL2 is involved in CCR2-mediated cochlear infiltration of monocytes (28). However, we poorly understand how the SLFs contribute to the recruitment of polymorphonuclear leukocytes (PMNs).

Among PMN-attracting chemokines, we showed that CXCL2, also known as macrophage inflammatory protein-2, is highly up-

^{*}Division of Clinical and Translational Research, House Research Institute, Los Angeles, CA 90057; and [†]Department of Cell and Neurobiology, Keck School of Medicine, University of Southern California, Los Angeles, CA 90089

¹S.O. and J.-I.W. contributed equally to this work.

Received for publication November 7, 2011. Accepted for publication February 1, 2012.

This work was supported in part by Grants DC8696, DC5025, and DC6276 from the National Institute on Deafness and Other Communication Disorders, National Institutes of Health.

Address correspondence and reprint requests to Dr. Sung K. Moon, House Research Institute, 2100 West 3rd Street, Los Angeles, CA 90057. E-mail address: smoon@hei.org

The online version of this article contains supplemental material.

Abbreviations used in this article: ALEX, alternating laser excitation; CHIP, chromatin immunoprecipitation; OM, otitis media; PMN, polymorphonuclear leukocyte; SLF, spiral ligament fibrocyte; SNHL, sensorineural hearing loss.

Copyright © 2012 by The American Association of Immunologists, Inc. 0022-1767/12/\$16.00

regulated in the SLFs in response to OM pathogens (14). CXCL2, which is associated with inflammatory diseases such as arthritis, glomerulonephritis, and sepsis (29–31), is upregulated by LPS through the activation of both NF- κ B and c-Jun in the murine macrophages (32). Pyrrolidine dithiocarbamate induces CXCL2 only via c-Jun-dependent signaling pathway (33), whereas Sp-1 is involved in CXCL2 upregulation in response to both CpG-oligodeoxynucleotide and LPS (34). Because these results suggest that a signaling pathway required for CXCL2 induction varies according to the proinflammatory signals, we aimed to determine a signaling pathway involved in nontypeable *H. influenzae*-induced CXCL2 upregulation in the SLFs.

In this study, we show that the MEK1-dependent phosphorylation of ERK2 is involved in nontypeable *H. influenzae*-induced CXCL2 upregulation in the SLFs. We demonstrate that the SLFs require c-Jun for the upregulation of CXCL2 in response to nontypeable *H. influenzae*, and two AP-1 motifs of CXCL2 function as a nontypeable *H. influenzae*-responsive element. In addition, we found that the proximal AP-1 motif has a higher binding affinity to nontypeable *H. influenzae*-activated c-Jun compared with that of the distal one. We expect that our findings will enable us to understand further the molecular pathogenesis of OM-induced inner ear inflammation and provide us with a novel strategy for the prevention of inner ear complication secondary to middle ear inflammation.

Materials and Methods

Reagents

PD98059, SP600125, AG126, and FR180204 were purchased from Calbiochem (San Diego, CA). SB203580 was purchased from Tocris (Ellisville, MO). Tanshinone IIA, NAD, and hemin were purchased from Sigma-Aldrich (St. Louis, MO). TaqMan primers and probes for rat CXCL2 (Rn00586403) and rat GAPDH (4352338E) were purchased from Applied Biosystems (Foster City, CA).

Bacterial culture and preparation of bacterial lysate

Nontypeable *H. influenzae* strain 12, originally a clinical isolate from the middle ear fluid of a child with acute OM, was used in this study (35). The nontypeable *H. influenzae* lysate was prepared as described previously (36). Briefly, a single colony of nontypeable *H. influenzae* was harvested from a chocolate agar plate, inoculated into 3 ml brain–heart infusion broth supplemented with NAD and hemin (both at 10 μ g/ml), and placed in a shaking incubator overnight. After addition of 50 ml fresh brain–heart infusion broth, bacteria were further grown for 4 h to a midlog phase ($A_{600} = 0.5$ – 0.7). The supernatant was discarded after centrifugation at $10,000 \times g$ for 10 min. The bacterial pellet was resuspended in 10 ml phosphate-buffered solution and sonicated to lyse bacteria. The lysate was then centrifuged at $10,000 \times g$ for 10 min, and the supernatant was collected. The protein concentration of the nontypeable *H. influenzae* lysate was determined using the BCA Protein Assay Kit (Pierce Biotechnologies, Rockford, IL).

Animal experiments

C57BL/6 and *Cxcr2*^{-/-} mice [B6.129S2(C)-*Cxcr2*^{tm1Mwm}] were purchased from The Jackson Laboratory (Bar Harbor, ME). All animal experiments were approved by the Institutional Animal Care and Use Committee of the House Research Institute. Live nontypeable *H. influenzae* (10^7 CFU) was suspended in 10 μ l saline and was transtympanically inoculated into the middle ear of young adult male mice using a 30-gauge needle and syringe under a surgical microscope. As a control, normal saline was inoculated with the same procedure. Animals were sacrificed 5 d after inoculation, and temporal bones were dissected. After fixation and decalcification, the temporal bones were embedded in paraffin and were serially sectioned through the midmodiolar plane at a thickness of 5 μ m. H&E staining was performed on every 10th to 20th section for the histological analysis.

For immunolabeling, endogenous peroxidase activity was quenched with incubation in 0.3% H₂O₂ for 30 min after tissue sections were deparaffinized and rehydrated through an identical series of graded xylene and alcohol solutions. Nonspecific binding sites were blocked by preincubation with a 1:10 dilution of horse serum for 1 h at room temperature. The

polyclonal rabbit anti-CXCL2 Ab (1:200; Santa Cruz Biotechnology, Santa Cruz, CA) was incubated with the sample for 1 h at room temperature. The sections were washed with phosphate-buffered solution three times and incubated with a 1:500 dilution of the biotinylated anti-rabbit IgG Ab (Vector Laboratories, Burlingame, CA) for 30 min at room temperature. Peroxidase was attached by the avidin–biotin complex method, and signals were detected with diaminobenzidine tetrahydrochloride.

Cell culture

The rat SLF cell line (RSL) (37) and murine primary SLFs were used in this study. The RSL cells were maintained in DMEM (Invitrogen, Carlsbad, CA) supplemented with 10% FBS, penicillin (100 U/ml), and streptomycin (0.1 mg/ml). Primary SLFs were cultured from explants of the mouse cochlear lateral walls as described (27). Briefly, mouse pups (P3–P6) were euthanatized in a CO₂ chamber and then decapitated. The cochlea was isolated with preservation of its normal structure after dissecting the inner ear from the skull base. After removal of the bony otic capsule, the spiral ligaments were separated from the surrounding tissue (stria vascularis, organ of Corti, and Reissner's membrane) using fine forceps. Explants of the spiral ligaments were plated onto the plastic culture dishes in DMEM supplemented with 10% FBS. After proliferation of the primary cells, the explants were removed. All subcultured cells were spindle-shaped and anchorage-dependent with expression of Ca²⁺ ATPase like a type 1 SLF (38). Primary cells of passage 5 or less were used in this study. All cells were maintained at 37°C in a humidified atmosphere of 5% CO₂ and 95% air.

Migration assays

After 4–6 h starvation, the RSL cells were exposed to the nontypeable *H. influenzae* lysate (0.1 μ g/ml) for 24 h, and the conditioned medium was collected. As a control, the conditioned medium of the RSL cells was separately collected without nontypeable *H. influenzae* exposure. Migration assays were performed using a 24-well plate with polycarbonate membrane inserts (Millipore, Billerica, MA) as described (28). Briefly, primary bone marrow cells were harvested from C57BL/6 or *Cxcr2*^{-/-} mice and were resuspended after washing. Contaminating monocytes were depleted by adherence (30 min at 37°C). Cell suspensions (1×10^6 cells/well) were added onto the insert, and the conditioned medium was added to the lower well. As a positive control, a recombinant CXCL2 (R&D Systems, Minneapolis, MN) was used. The conditioned medium from the nontypeable *H. influenzae*-unexposed RSL cells was used as a negative control. Cells were allowed to migrate for 6 to 18 h at 37°C. After cyto-spin preparation and Giemsa staining, migrated PMNs were identified. Migrated cells were counted using a hemocytometer, and a fold-change was determined after normalization with the group of the conditioned medium from the nontypeable *H. influenzae*-unexposed RSL cells.

ELISA

CXCL2 protein levels in the conditioned medium from the RSL cells were measured using rat CXCL2 ELISA kits (RayBiotech, Norcross, GA) following the manufacturer's instructions.

Quantitative RT-PCR

Quantitative RT-PCR was performed as described previously (27). Briefly, the RSL cells were exposed to the nontypeable *H. influenzae* lysate, and total RNA was extracted using TRIzol reagent (Invitrogen). After cDNA was synthesized using the TaqMan Reverse Transcription Kit (Applied Biosystems), multiplex PCR was performed using the ABI 7500 Real-Time PCR system (Applied Biosystems) with gene-specific primers (FAM-conjugated probes for CXCL2) and control primers (a VIC-conjugated probe for GAPDH). The cycle threshold (C_T) values were determined according to the manufacturer's instructions, and the relative quantity of mRNA was determined using the 2^{- $\Delta\Delta$ CT} method (39). C_T values were normalized to the internal control (GAPDH), and the results were expressed as a fold change of mRNA with the mRNA levels in the nontreated group set as 1.

Plasmids, transfections, and luciferase assays

The vectors expressing a dominant-negative construct of MEK1 (K97R), a wild-type construct of MEK1, a dominant-negative construct of ERK1 (K71R), a dominant-negative construct of ERK2 (T183A/Y185F), and a dominant-negative construct of c-Jun (TAM67) were previously described (40–43). Promoter fragments (–3475 to +14, –563 to +14, and –134 to +14) of the rat CXCL2 (NM_053647) were amplified, and KpnI and XhoI sites were added with the following primers: 5'-AGGTACCTTTGCC-

CACTGGCAAGCCTACCAAGGCCTCTAC-3' (-3475); 5'-CGGGTAC-CAGGATATGACACAAAA-3' (-563); 5'-CGGTACCTACTCAGCTC-TCGGGG-3' (-134); and 5'-GCTCGAGGGGCCATGGCGCT-3' (+14). Each fragment was ligated into KpnI and XhoI sites of the pGL3 luciferase reporter plasmid (Promega, Madison, WI), and constructs were verified by sequencing. The luciferase-expressing constructs containing the promoter region of the mouse CXCL2 (NM_009140) were provided by Dr. Hyung-Joo Kwon (Hallym University, Chuncheon, Korea) (32). Constructs were transfected to cells using the Transit-LT1 transfection reagent (Mirus, Madison, WI) according to the manufacturer's instructions. The pRL-TK vector (Promega) was cotransfected to normalize transfection efficiency. Transfected cells were then starved overnight in serum-free DMEM, followed by exposure to the nontypeable *H. influenzae* lysate for 8 h before harvesting. All transfections were carried out in triplicate. After washing with PBS, cells were dissolved in the lysis reagent (Promega). Luciferase activity was measured using a luminometer (Pharmingen) after adding the necessary luciferase substrate (Promega). Results were expressed as a fold change of luciferase activity, taking the value of the nontreated group as 1.

Site-directed mutagenesis

To introduce site-specific mutations to the AP-1 motifs in the 5'-flanking region of the rat CXCL2, site-directed mutagenesis was performed with the QuikChange II XL Site-Directed Mutagenesis Kit (Agilent Technologies, Santa Clara, CA). Briefly, PCR was conducted to replicate mutagenic plasmids using the following primers: 5'-CCTTAATTCTCCAGTCC-TAATGGTACCAGTCTCTCAAACCTGTTG-3' for the distal AP-1 motif and 5'-GAAGGGCAGGGAAGTATGATGGGTACCGCATTCATGCG-TGCACG-3' for the proximal AP-1 motif (boldface: mutated bases). To digest completely parental template plasmids, 10 U of a methylation-sensitive restriction enzyme, DpnI, was added to the PCR products and incubated overnight at 37°C. The mutated plasmids were transformed into *Escherichia coli* XL10-Gold, and the transformation mixture was plated on lysogeny broth medium containing ampicillin. After preparation of plasmids, point mutations were identified with sequencing.

Phosphorylation assays

Cells were grown to 80% confluence in 6-well culture plates. After overnight starvation with basal medium, cells were treated with the nontypeable *H. influenzae* lysate for 3, 5, 10, 20, 40, and 60 min. Cells were lysed with cell lysis buffer (Cell Signaling Technology, Danvers, MA) supplemented with a protease inhibitor mixture and 1 mM PMSF (Calbiochem). The lysates were then centrifuged at $14,000 \times g$ for 15 min, and the supernatants were collected. For c-Jun, the nuclear proteins were collected using Nuclear Extract Kit (Active Motif) according to the manufacturer's instructions. After measurement of protein concentrations of supernatants, an amount equivalent to 20 µg of proteins was loaded onto 10% Tricine gels (Invitrogen), and electrophoresis was conducted in a Tris-Tricine-NaDodSO₄ tank buffer (pH 7.4). After electrophoresis, proteins were transferred onto polyvinylidene difluoride membranes (Bio-Rad, Hercules, CA) and washed three times for 5 min each in TBS plus 0.05% Tween 20 (TBST). Membranes were blocked using 5% nonfat dry milk in TBST for 1 h at room temperature and incubated overnight at 4°C in the presence of a 1:1000 dilution of a polyclonal Ab against phosphorylated ERK1/2 and c-Jun and against total ERK1/2 and c-Jun (Cell Signaling Technology). After washing, membranes were incubated with an HRP-conjugated secondary Ab in a blocking buffer. Membranes were then incubated with a SuperSignal substrate (Pierce Biotechnologies) for 1 min at room temperature, and chemiluminescence signals were detected by exposure to x-ray films.

Transcription factor assays

Nontypeable *H. influenzae*-activated transcription factors were analyzed using the ELISA-based TransAM kit (Active Motif, Carlsbad, CA) as described (27). In brief, after the nuclear proteins were extracted from the RSL cells using Nuclear Extract Kit (Active Motif), nuclear proteins were applied to a 96-well plate coated with oligonucleotides containing the consensus sequences of various transcription factors. To demonstrate a binding specificity, binding activities of transcription factors were inhibited with a competitor, unbound consensus oligonucleotides. After washing, bound transcription factors were labeled with a 1:1000 dilution of primary polyclonal Abs against each transcription factor at room temperature for 1 h. Unbound Abs were washed out, and wells were incubated with a 1:1000 dilution of anti-rabbit IgG conjugated with HRP at room temperature for 30 min. One hundred microliters of tetramethylbenzidine substrate was added to each well and incubated at room temperature for 10 min. The absorbance was measured at 450 nm with a microplate reader.

Chromatin immunoprecipitation

The RSL cells were treated with the nontypeable *H. influenzae* lysate in the presence or absence of MEK inhibitor and fixed with 1% formaldehyde for 10 min. After lysis of cells with 1 ml of an ice-cold lysis buffer supplemented with a protease inhibitor mixture and PMSF, the nuclear fraction was collected using Nuclear Extract Kit (Active Motif). After resuspending of the nuclear extract, enzymatic shearing of chromatin was conducted. The sheared DNA samples were centrifuged at $15,000 \times g$ for 10 min at 4°C, and the supernatant was collected ("Input DNA"). Input DNA samples were incubated with 3 µg/ml of an anti-phosphorylated c-Jun Ab and 25 µl of protein G magnetic beads overnight at 4°C. The samples were placed on the magnetic stand to pellet beads, and the supernatant was discarded carefully. After washing, the pelleted beads were resuspended and named as chromatin immunoprecipitation DNA ("ChIP DNA"). To reverse cross-links, ChIP DNA samples and Input DNA samples were incubated at 65°C for 2.5 h and then were mixed with 1 µg/µl proteinase K and incubated at 37°C for 1 h. Conventional PCR and quantitative PCR was performed on Input DNA and ChIP DNA samples using the following primer pairs: 5'-TATGTAACTAACGGAGACGCACCC-3' and 5'-AAAC-CCTCAGGAGGAAGGAAGTGA-3' (distal AP-1 motif, 190 bp); and 5'-TTGTCTGCCTGATGACATCGCT-3' and 5'-TTAGGGTCCCTGCAT-CAGGAAGAA-3' (proximal AP-1 motif, 230 bp).

Alternating laser excitation fluorescence spectroscopy

Alexa 647N-labeled 21-mer double-stranded oligonucleotides containing the proximal and distal AP-1 motifs of the rat CXCL2 were prepared (IDT, Coralville, IA). The RSL cells were treated with nontypeable *H. influenzae* lysate and lysed with cell lysis buffer. After extraction of nuclear fractions, samples were purified using Microcon (Ambion, Foster City, CA) to remove detergents and salts. Samples were resuspended in a Tris buffer (pH 7.5) and were incubated with Alexa 647N-labeled oligonucleotides overnight at 4°C (an acceptor). Samples were washed and incubated with an Alexa 488-labeled Ab against phosphorylated c-Jun (Cell Signaling Technology) overnight at 4°C (a donor). In collaboration with Neshor Technologies (Los Angeles, CA), alternating laser excitation (ALEX) fluorescence spectroscopy was performed as previously described (44–46). Briefly, the donor was directly excited by the first laser (488 nm), and the acceptor-derived emission (669 nm) was detected with and without the second laser (647 nm). Donor-acceptor stoichiometry was analyzed with normalization of burst counts by total burst counts of the consistent areas on the FRET efficiency and stoichiometry diagram.

Statistics

All experiments were carried out in triplicate and repeated twice. Results were expressed as means \pm SDs. Statistical analysis was performed using Student *t* test and ANOVA followed by Tukey's post hoc test using the R2.14.0 software for Window (The R Foundation for Statistical Computing). A *p* value <0.05 was considered significant.

Results

SLFs upregulate CXCL2 in response to nontypeable *H. influenzae*-induced middle ear infection

In the prior study, we demonstrated that the SLFs release MCP-1/CCL2 in response to nontypeable *H. influenzae*, resulting in cochlear recruitment of monocytes (28). In addition to monocytes, our animal model for OM-induced inner ear inflammation showed that transtympanic inoculation of live nontypeable *H. influenzae* leads to cochlear infiltration of PMNs (Supplemental Fig. 1A). Based on the finding that the SLFs are able to release various cytokines and chemokines in response to proinflammatory signals (13), we sought to determine if nontypeable *H. influenzae*-induced SLF-derived molecules attract PMNs. As shown in Fig. 1A, the SLFs appeared to release CXCR2 ligands resulting in migration of PMNs. Among the CXCR2 ligands, we focused on CXCL2 because we found that the SLFs upregulate CXCL2 in response to nontypeable *H. influenzae* in the rats and mice (14) (Supplemental Fig. 1C). Next, we performed ELISA analysis to show nontypeable *H. influenzae*-induced regulation of CXCL2 at the protein levels. In accord with our previous findings (14), the RSL cells were found to upregulate CXCL2 upon exposure to nontypeable *H. influenzae* in

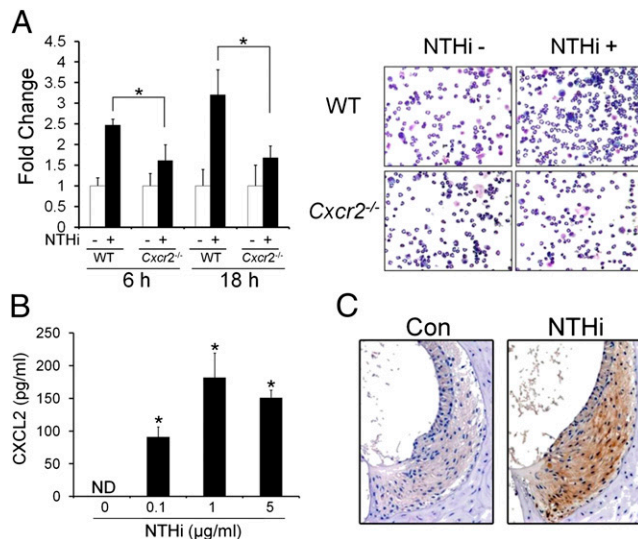


FIGURE 1. SLFs upregulate CXCL2 in response to nontypeable *H. influenzae*. **(A)** Migration assays show that CXCR2 deficiency inhibits migration of PMNs in response to the nontypeable *H. influenzae*-induced SLF-derived molecules. WT, wild-type PMNs; *Cxcr2*^{-/-}, CXCR2-deficient PMNs; NTHi, nontypeable *H. influenzae*; NTHi⁻, conditioned medium from the nontypeable *H. influenzae*-unexposed RSL cells; NTHi⁺, conditioned medium from the nontypeable *H. influenzae*-exposed RSL cells. **(B)** ELISA analysis shows that the RSL cells upregulate CXCL2 in response to nontypeable *H. influenzae*. ND, not detected. The experiments were performed in triplicate and repeated twice. Values are given as the mean \pm SD ($n = 3$). * $p < 0.05$. **(C)** Immunohistochemistry with diaminobenzidine shows that CXCL2 is highly expressed in the spiral ligament of the nontypeable *H. influenzae*-inoculated mice (NTHi), but not in the saline-inoculated mice (Con). Original magnification $\times 50$.

a dose-dependent manner (Fig. 1B). To determine if CXCL2 is associated with OM-induced inner ear inflammation in vivo, immunolabeling of the murine temporal bone was performed using an anti-CXCL2 Ab after transtympanic inoculation of live nontypeable *H. influenzae*. As shown in Fig. 1C, CXCL2 was highly expressed in the spiral ligament of the nontypeable *H. influenzae*-inoculated mice compared with that in the spiral ligament of the saline-inoculated mice. Transtympanic inoculation of nontypeable *H. influenzae* was found to induce middle ear inflammation with mucosal thickening, which was resolved within 7 d (data not shown). OM-induced inner ear inflammation was noted 5–6 d after nontypeable *H. influenzae* inoculation and remained after resolution of middle ear inflammation, indicating that inner ear inflammation is secondary to OM. Taken together, it is suggested that the SLFs are critically involved in cochlear infiltration of PMNs secondary to nontypeable *H. influenzae*-induced OM.

Activation of c-Jun is required for nontypeable *H. influenzae*-induced CXCL2 upregulation

Based on the requirement of NF- κ B for nontypeable *H. influenzae*-induced upregulation of MCP-1/CCL2 in the SLFs (27) and LPS-induced CXCL2 upregulation in the murine macrophages (32, 33), we predicted that NF- κ B is also involved in CXCL2 induction in response to nontypeable *H. influenzae*. Unexpectedly, quantitative RT-PCR analysis and ELISAs showed that inhibition of NF- κ B signaling insignificantly suppresses nontypeable *H. influenzae*-induced CXCL2 upregulation in the RSL cells (Supplemental Fig. 2), suggesting the involvement of NF- κ B-independent signaling pathways. Because transcriptional regulation of CXCL2 is known to vary according to the proinflammatory signals (32, 33, 47), we sought to explore transcription factors involved in nontypeable *H.*

influenzae-induced CXCL2 upregulation using transcription factor ELISAs. The RSL cells were found to activate c-Jun in response to nontypeable *H. influenzae*, leading to selective binding to the consensus sequences of AP-1 motifs (Fig. 2A). Moreover, phosphorylation assays showed nontypeable *H. influenzae*-induced phosphorylation of nuclear c-Jun (Fig. 2B). We next sought to determine if nontypeable *H. influenzae*-induced c-Jun activation requires nontypeable *H. influenzae*-induced CXCL2 upregulation. As shown in Fig. 2C, Tanshinone IIA, a c-Jun phosphorylation inhibitor, appeared to suppress nontypeable *H. influenzae*-induced CXCL2 upregulation in a dose-dependent manner. To determine further the involvement of c-Jun, luciferase assays were performed using a luciferase-expressing reporter containing the 5'-flanking region of the rat CXCL2 after the RSL cells were cotransfected with the dominant-negative construct of c-Jun (TAM67). As shown in Fig. 2D, nontypeable *H. influenzae*-induced upregulation of CXCL2 transcription was inhibited by TAM67. Consistently, ELISA analysis showed that TAM67 markedly suppresses nontypeable *H. influenzae*-induced upregulation of CXCL2 translation (Fig. 2E), suggesting that the activation of c-Jun is required for nontypeable *H. influenzae*-induced CXCL2 upregulation.

MEK1/ERK2 signaling pathway is involved in nontypeable *H. influenzae*-induced CXCL2 upregulation in SLFs

To determine upstream signaling molecules involved in nontypeable *H. influenzae*-induced c-Jun-mediated CXCL2 upregulation, RSL cells were pretreated with chemical inhibitors of the MAPKs. Notably, nontypeable *H. influenzae*-induced CXCL2 upregulation was markedly inhibited only by PD98059, but not by other MAPK inhibitors (Fig. 3A). To investigate further the involvement of MEK1, the RSL cells were transfected with a dominant-negative construct of MEK1. In accord with the inhibitor study, a dominant-negative inhibition of MEK1 appeared to suppress nontypeable *H. influenzae*-induced CXCL2 upregulation. In contrast, overexpression of a wild-type MEK1 enhanced nontypeable *H. influenzae*-induced CXCL2 upregulation (Fig. 3B). Because ERKs are downstream molecules of MEK1, we sought to determine the involvement of ERK1/2 in nontypeable *H. influenzae*-induced CXCL2 upregulation. As expected, pretreatment with AG126 (an MEK inhibitor) and FR180204 (an ERK inhibitor) significantly inhibited nontypeable *H. influenzae*-induced CXCL2 upregulation (Fig. 3C). Next, we performed phosphorylation assays to determine nontypeable *H. influenzae*-induced ERK activation. Notably, only ERK2, not ERK1, was phosphorylated upon exposure to nontypeable *H. influenzae*, peaking 10 min later (Fig. 3D). To dissect functions of each ERK isoform further, ERK expression was suppressed by a dominant-negative construct of ERK1 or ERK2. In accord with the finding of the phosphorylation assays, nontypeable *H. influenzae*-induced CXCL2 upregulation was found to be inhibited only by a dominant-negative construct of ERK2, but not by ERK1 (Fig. 3E). Consistently, ELISA analysis showed that a dominant-negative inhibition of ERK2 markedly suppresses nontypeable *H. influenzae*-induced CXCL2 upregulation (Fig. 3F). Next, we sought to determine if nontypeable *H. influenzae*-induced c-Jun activation requires the MEK-dependent signaling pathway. As shown in Fig. 3G, MEK inhibitors such as PD98059 and AG126 appeared to suppress nontypeable *H. influenzae*-induced activation of c-Jun. These results suggested that MEK1/ERK2-mediated activation of c-Jun is involved in nontypeable *H. influenzae*-induced CXCL2 upregulation in the SLFs.

Identification of a nontypeable *H. influenzae*-responsive AP-1 motif of CXCL2

To determine nontypeable *H. influenzae*-responsive elements in the 5'-flanking region of CXCL2, the luciferase-expressing con-

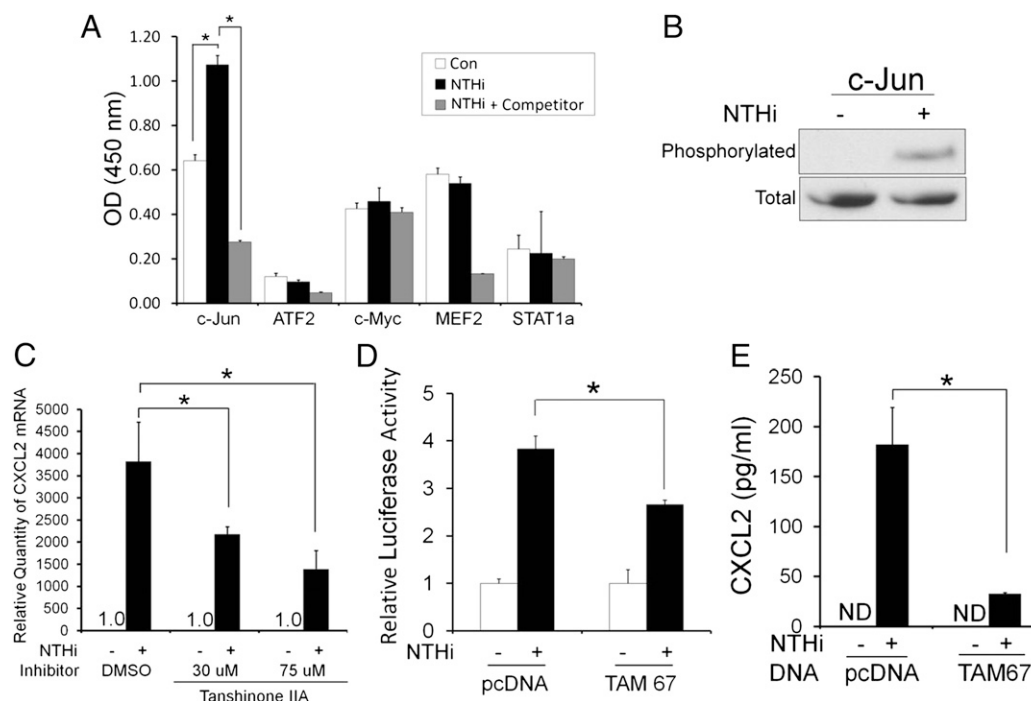


FIGURE 2. Activation of the c-Jun is required for nontypeable *H. influenzae*-induced CXCL2 upregulation. **(A)** Transcription factor ELISAs show that the SLFs activate c-Jun in response to nontypeable *H. influenzae*. **(B)** Phosphorylation assays show that c-Jun of the nuclear fraction is phosphorylated in response to nontypeable *H. influenzae*. **(C)** Nontypeable *H. influenzae*-induced CXCL2 upregulation is noted to be inhibited by Tanshinone IIA in a dose-dependent manner. **(D)** Luciferase assays demonstrate that a dominant-negative inhibition of c-Jun (TAM 67) suppresses nontypeable *H. influenzae*-induced CXCL2 upregulation. **(E)** ELISA analysis shows that a dominant-negative inhibition of c-Jun (TAM 67) markedly suppresses nontypeable *H. influenzae*-induced CXCL2 upregulation. Results were expressed as fold-induction, taking the value of the nontreated group as 1. The experiments were performed in triplicate and repeated twice. Values are given as the mean \pm SD ($n = 3$). * $p < 0.05$. NTHi, nontypeable *H. influenzae*; ND, not detected; pcDNA, a mock transfection.

structs containing the nested deletions of the 5'-flanking region of the rat CXCL2 were generated. Luciferase assays showed that the 134-bp construct has the least promoter activity compared with that of the 3475-bp and 563-bp constructs (Fig. 4A), indicating that the nontypeable *H. influenzae*-responsive elements exist between -563 bp and -134 bp of the 5'-flanking region of the rat CXCL2. The motif analysis of this region predicted two AP-1 motifs, which agreed with the previous studies showing that two AP-1 motifs exist in the 5'-flanking region of the mouse CXCL2 (32). To determine the requirement of these AP-1 motifs for nontypeable *H. influenzae*-induced CXCL2 upregulation in the SLFs, we conducted site-directed mutagenesis. As shown in Fig. 4B, nontypeable *H. influenzae*-induced CXCL2 upregulation was inhibited by the mutation of each AP-1 motif, and the mutation of both sites completely inhibited CXCL2 induction. Notably, the proximal AP-1 motif appeared to be more involved in nontypeable *H. influenzae*-induced CXCL2 upregulation than the distal one. In the mouse CXCL2, both AP-1 motifs were also found to be involved in nontypeable *H. influenzae*-induced upregulation of CXCL2 expression (Supplemental Fig. 3).

Nontypeable *H. influenzae*-activated c-Jun binds the AP-1 motif of CXCL2

Next, we sought to determine if nontypeable *H. influenzae*-activated c-Jun binds the AP-1 motifs of the rat CXCL2. We performed ChIP-PCR assays using an anti-c-Jun Ab and the primers spanning either distal or proximal AP-1 motif of CXCL2. Nontypeable *H. influenzae*-activated c-Jun was found to bind both distal and proximal AP-1 motifs of the rat CXCL2 (Fig. 5A). We further investigated if the MEK-dependent signaling pathway is involved in nontypeable *H. influenzae*-induced binding of c-Jun to

both AP-1 motifs of the rat CXCL2. As shown in Fig. 5B, PD98059 significantly inhibited nontypeable *H. influenzae*-induced binding of c-Jun to both distal and proximal AP-1 motifs of CXCL2. Alignment analysis showed that three bases of the 3' side are different between the proximal and distal AP-1 motifs (Fig. 6A). In addition, two AP-1 motifs were found to have only two bases in common out of seven bases flanking the core recognition site in each side. To determine if this sequence difference leads to a difference in the binding affinity of the AP-1 motifs to nontypeable *H. influenzae*-activated c-Jun in vitro, ALEX fluorescence spectroscopy was performed using the Alexa 647N-labeled DNA fragments containing each AP-1 motif and the Alexa 488-labeled Ab against c-Jun. Notably, only the proximal AP-1 motif, not the distal one, showed 2.13 ± 0.53 -fold increase in ALEX efficiency (Fig. 6B). This result indicated that the proximal AP-1 motif has a higher binding affinity to nontypeable *H. influenzae*-activated c-Jun than that of the distal one in vitro, agreeing with our site-directed mutagenesis study. Taken together, it is suggested that MEK-dependent activation of c-Jun is required for nontypeable *H. influenzae*-induced binding of c-Jun to the proximal AP-1 binding motif of CXCL2, resulting in upregulation of CXCL2 expression.

Discussion

In this study, we showed that the SLFs upregulate CXCL2 in response to nontypeable *H. influenzae* via ERK2-dependent activation of c-Jun, which is involved in inner ear inflammation secondary to OM. We also found that binding of c-Jun to the AP-1 motifs, particularly to the proximal one, in the 5'-flanking region of CXCL2 is required for nontypeable *H. influenzae*-induced CXCL2 upregulation. Furthermore, we demonstrated a higher

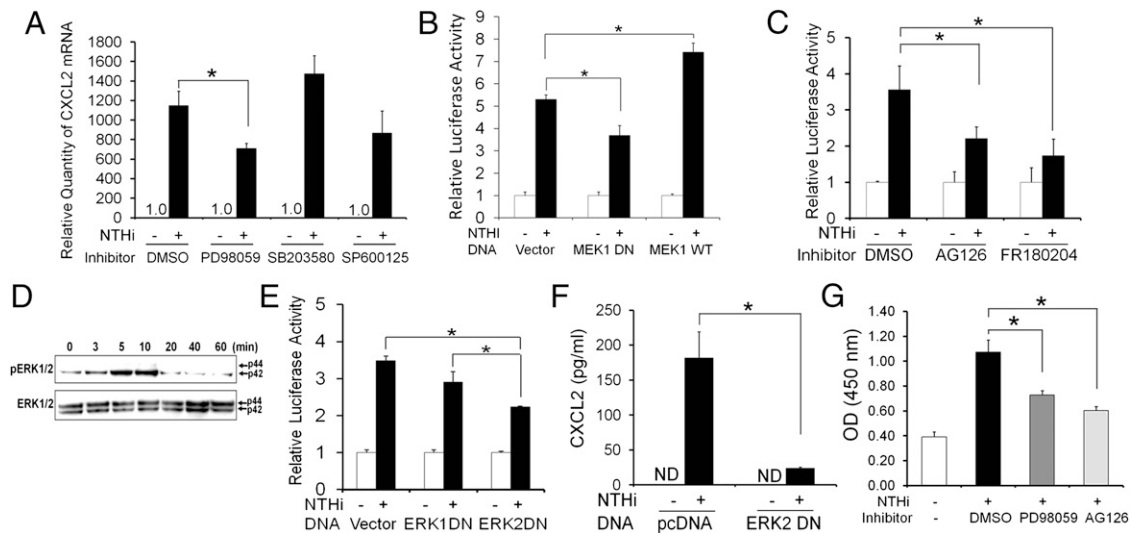


FIGURE 3. MEK1/ERK2 signaling is required for nontypeable *H. influenzae*-induced activation of c-Jun resulting in CXCL2 upregulation in SLFs. **(A)** Quantitative RT-PCR analysis shows that nontypeable *H. influenzae*-induced CXCL2 upregulation is inhibited by PD98059, a MEK inhibitor, but not by other MAPK inhibitors. **(B)** Luciferase assays demonstrate that a dominant-negative inhibition of MEK1 suppresses nontypeable *H. influenzae*-induced CXCL2 upregulation but is enhanced by the overexpression of the wild type of MEK1. Vector, a mock transfection. **(C)** Nontypeable *H. influenzae*-induced CXCL2 upregulation is noted to be inhibited by AG126 and FR180204. **(D)** Phosphorylation assays show that the SLFs activate ERK in response to nontypeable *H. influenzae*, peaked around 10 min after exposure. Note that ERK2 (p42), not ERK1 (p44), is mainly phosphorylated upon exposure to nontypeable *H. influenzae* in the SLFs. **(E)** Luciferase assays show that nontypeable *H. influenzae*-induced CXCL2 upregulation is suppressed by a dominant-negative inhibition of ERK2, but not by ERK1. **(F)** ELISA analysis shows that a dominant-negative inhibition of ERK2 significantly suppresses nontypeable *H. influenzae*-induced CXCL2 upregulation. ND, not detected; pcDNA, a mock transfection. **(G)** Transcription factor ELISAs show that nontypeable *H. influenzae*-induced activation of c-Jun is inhibited by PD98059 and AG126. Results were expressed as fold-induction, taking the value of the nontreated group as 1. The experiments were performed in triplicate and repeated twice. Values are given as the mean \pm SD ($n = 3$). $*p < 0.05$. NTHi, nontypeable *H. influenzae*.

binding affinity of the proximal AP-1 motif to nontypeable *H. influenzae*-activated c-Jun.

PMNs are a major element of the innate immune defense against invading pathogens, but their overly robust response can lead to pathological sequelae from local tissue damage to organ dysfunction. Because OM-induced cochlear infiltration of PMNs is believed to contribute to OM-induced SNHL (48), it is important to understand the molecular mechanism involved in the cochlear infiltration of PMNs in response to middle ear inflammation. In this study, we showed that fibrocytes of the cochlear spiral ligament release PMN-attracting CXCR2 ligands in response to nontypeable *H. influenzae*. In humans, IL-8 (CXCL8) is a major PMN chemoattractive agent (49–51), whereas CXCL1 and CXCL2 are known to serve mainly as CXCR2 ligands leading to chemoattraction of PMNs in rodents. Although the RSL cells are suggested to release a variety of PMN-attracting molecules in response to nontypeable *H. influenzae* (Supplemental Fig. 1B), we further focused on CXCL2 regulation based on the findings that CXCL2 is more active than CXCL1 in recruiting PMNs (52–54).

CXCL2 was first identified as a major heparin-binding protein secreted from the endotoxin-stimulated murine macrophages (55). Besides a potent chemoattractive activity for PMNs, animal experiments showed the role of CXCL2 in regulation of ischemia-induced leukocyte adhesion (56) and sepsis-mediated lung injury (57). Furthermore, CXCL2 was found to be involved in proliferation and protection of hepatocytes (58, 59), pulmonary angiogenesis and fibrosis (60), osteoclastogenesis (61), hepatic metastasis of colorectal cancer cells (62), and stem cell mobilization (63) in animal studies. In humans, CXCL2 was discovered as one of the GRO genes having a growth-stimulating activity (64). CXCL2 is clinically a potential cancer marker because CXCL2 dysregulation is frequently found in patients with esophageal carcinoma (65), non-small cell lung cancer (66), and colon cancer (67). In addition,

a CXCL2 polymorphism is known to be associated with higher mortality of sepsis (68). The role of CXCL2 in inner ear inflammation is poorly understood, but we here demonstrated the molecular mechanism involved in contribution of SLF-derived CXCL2 to OM-induced inner ear inflammation.

Transcription of CXCL2 is known to be regulated by the NF- κ B- and/or c-Jun-dependent signaling. LPS induces CXCL2 via both NF- κ B- and c-Jun-dependent regulation in the mouse macrophage cell line (32), whereas pyrrolidine dithiocarbamate-induced CXCL2 upregulation is NF- κ B independent but c-Jun dependent (33). In addition, oligodeoxynucleotide containing CpG motif is known to upregulate CXCL2 only via NF- κ B activation (47). Unlike other Gram-negative bacteria, nontypeable *H. influenzae* contains atypical LPS; that is, lipo-oligosaccharides lacking an O-specific polysaccharide in the outer membrane (69). In contrast to LPS, this study showed that nontypeable *H. influenzae* upregulates CXCL2 only via c-Jun activation mediated by ERK2 phosphorylation.

The AP-1 complex, a dimer of Jun, Fos, and ATF family members binding AP-1 motifs, is involved in activation of genes associated with various cellular events such as proliferation, differentiation, and apoptosis (70, 71). A heterodimer of c-Jun and c-Fos is known to serve most frequently as an AP-1 complex (72). c-Jun can form a homodimer, whereas Fos proteins usually do not form a homodimer (73). In agreement with our previous report showing that c-Fos is not highly activated in response to nontypeable *H. influenzae* (27), a dominant-negative construct of c-Fos (A-Fos) did not inhibit the nontypeable *H. influenzae*-induced CXCL2 upregulation (data not shown). These results suggest that the nontypeable *H. influenzae*-activated AP-1 complex is either a c-Jun homodimer or a c-Jun heterodimer with other AP-1 components than c-Fos. Generally, c-Jun is known to be activated by a JNK-mediated signaling pathway. However, our results showed ERK2, not JNK,

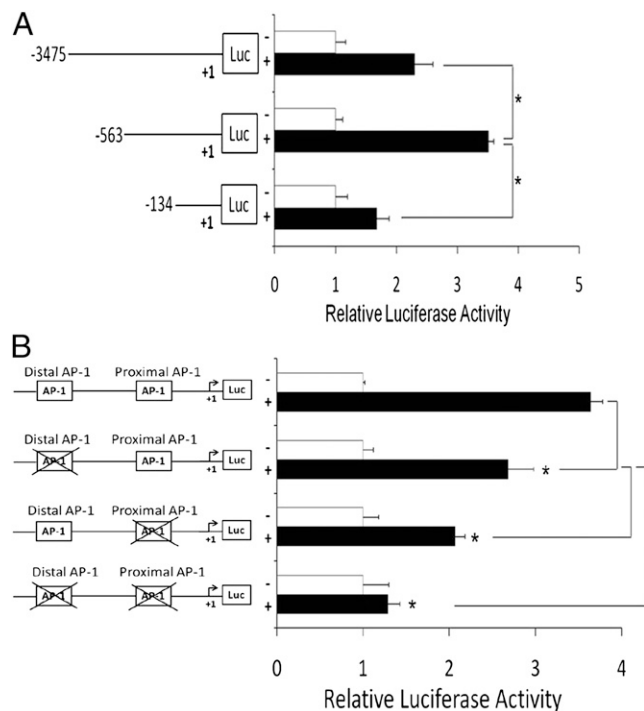


FIGURE 4. The AP-1 motif is critically involved in nontypeable *H. influenzae*-induced CXCL2 upregulation. **(A)** Luciferase assays using nested deletions show that the nontypeable *H. influenzae*-responsive element is located between -564 and -134 of the rat CXCL2 promoter region. **(B)** Luciferase assays with site-directed mutagenesis show that the mutation of the proximal AP-1 motif inhibits nontypeable *H. influenzae*-induced CXCL2 upregulation more than that by mutation of the distal AP-1 motif. Mutation of both AP-1 motifs is noted completely to inhibit nontypeable *H. influenzae*-induced CXCL2 upregulation. Results were expressed as fold-induction, taking the value of the nontreated group as 1. The experiments were performed in triplicate and repeated twice. Values are given as the mean \pm SD ($n = 3$). $*p < 0.05$.

is critically involved in nontypeable *H. influenzae*-induced CXCL2 upregulation. In agreement with our result, *Helicobacter pylori* induces apoptosis in macrophages via ERK-dependent activation of c-Jun (71). In addition, ERK-dependent c-Jun activation is known to induce neuronal differentiation, whereas JNK-mediated c-Jun activation is involved in induction of apoptosis (74), suggesting that the upstream molecules involved in c-Jun activation affect c-Jun-mediated cellular events.

Furthermore, we found that ERK2, not ERK1, is strongly involved in nontypeable *H. influenzae*-induced CXCL2 upregulation in the SLFs. Specific functions of each ERK isoform remain unclear, but functional redundancy has been a working model, as ERK isoforms are 90% identical to each other (75) and share activators and substrates. However, there is emerging evidence showing that ERK1 and ERK2 have different functions. Deficiency of ERK2 results in early embryonic death due to a placental defect (76), but the lack of ERK1 does not influence growth and reproduction of mice (77). Silencing of ERK2 appeared completely to suppress cell proliferation, whereas ERK1 deficiency resulted in a growth advantage associated with an enhancement of ERK2-dependent signaling (78). ERK is known to be required for nontypeable *H. influenzae*-induced IL-8 production in human epithelial cells (79), but only one of the ERK isoforms was noted to be phosphorylated upon exposure to nontypeable *H. influenzae*. Our study indicates that the nontypeable *H. influenzae*-activated ERK isoform is ERK2 resulting in CXCL2

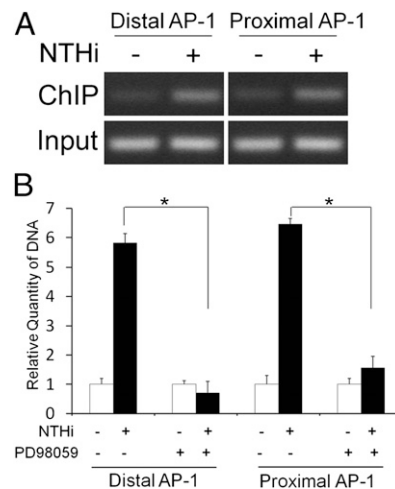


FIGURE 5. Nontypeable *H. influenzae*-activated c-Jun binds the AP-1 motifs of CXCL2. **(A)** ChIP-PCR analysis shows that c-Jun binds the AP-1 motifs of CXCL2 in response to nontypeable *H. influenzae*. **(B)** ChIP-quantitative PCR analysis shows that PD98059 inhibits nontypeable *H. influenzae*-induced binding of c-Jun to both AP-1 motifs. Results were expressed as fold-induction, taking the value of the nontreated group as 1. The experiments were performed in triplicate and repeated twice. Values are given as the mean \pm SD ($n = 3$). $*p < 0.05$. NTHi, nontypeable *H. influenzae*.

induction, which will bring a new insight into a novel role of the ERK2 isoform in bacterial infections.

TLR2 is known to play an important role in recognition of nontypeable *H. influenzae* molecules in epithelial cells (80). We also demonstrated that the SLFs upregulate MCP-1/CCL2 in response to nontypeable *H. influenzae* via TLR2/MyD88 signaling (27). Consistently, we found that TLR2 and MyD88 are involved in nontypeable *H. influenzae*-induced CXCL2 upregulation in the SLFs (Supplemental Fig. 4). This result suggests that ERK signaling mediates nontypeable *H. influenzae*-induced TLR2 signal-

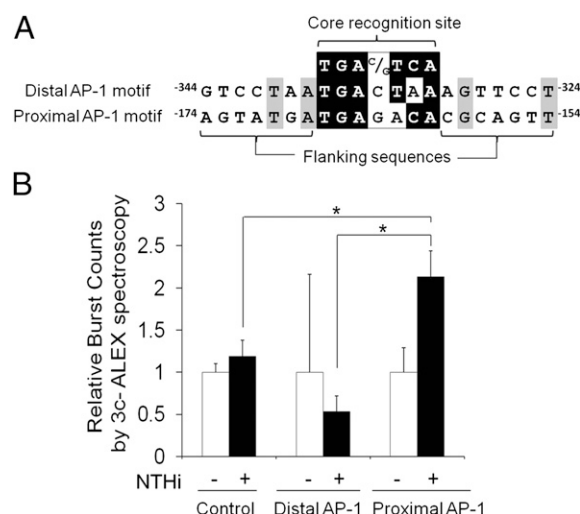


FIGURE 6. The proximal AP-1 motif has a higher binding affinity to c-Jun/DNA binding than that of the distal one in vitro. **(A)** Sequence alignment analysis showing a difference between the distal and proximal AP-1 motifs. **(B)** ALEX fluorescence spectroscopy shows that the proximal AP-1 motif has a higher binding affinity to nontypeable *H. influenzae* (NTHi)-activated c-Jun than that of the distal one in vitro. Results were expressed as fold-induction, taking the value of the nontreated group as 1. The experiments were performed in triplicate and repeated twice. Values are given as the mean \pm SD ($n = 3$). $*p < 0.05$.

ing although nontypeable *H. influenzae*-induced TLR2 signaling is known to be transmitted mainly through p38 MAPKs (81–83). Similarly, TLR2-dependent ERK activation has been reported to be involved in bacterial teichoic acid-induced upregulation of IL-10 (84) and inducible NO synthase (85) and hepatitis C virus-induced neurotoxic effects (86). Moreover, transient hypoxia of the kidney cells is known to induce TLR2-mediated activation of ERK (87).

Although ChIP analysis showed that nontypeable *H. influenzae*-activated c-Jun binds both distal and proximal AP-1 motifs of CXCL2, ALEX fluorescence spectroscopy demonstrated that the proximal AP-1 motif has a higher binding affinity to nontypeable *H. influenzae*-activated c-Jun than that of the distal one. Consistent with the finding of ALEX fluorescence spectroscopy, site-directed mutagenesis revealed that the proximal AP-1 motif contributes to nontypeable *H. influenzae*-induced CXCL2 upregulation more than the distal one. The AP-1 motif is asymmetric from the central C:G base pair, but binding of AP-1 is orientation independent (88). Sequences flanking the conserved AP-1 core recognition site also affect the affinity of AP-1 binding (89, 90) through the influencing of DNA bending (91). Difference in core recognition sequences and flanking sequences of two AP-1 motifs of CXCL2 may contribute to difference in the binding affinity of two AP-1 motifs, but further studies are needed to reveal a key sequence involved in a higher binding affinity of the proximal one.

In conclusion, we demonstrated that the SLFs play a central role in inner ear inflammation by upregulation of CXCL2 through c-Jun activation mediated by a MEK1/ERK2-dependent signaling pathway. SLF-derived CXCL2 is suggested to recruit PMNs to the cochlea, and inflammation-associated tissue damage is believed to contribute to OM-induced inner ear dysfunction such as SNHL. Our study will bring an insight into the molecular pathogenesis of OM-induced inner ear dysfunction and provide a novel strategy for the prevention of inner ear complication secondary to middle ear inflammation.

Acknowledgments

We thank Drs. Nancy Colburn (National Cancer Institute, National Institutes of Health), Jian-Dong Li (Georgia State University), and Hyung-Joo Kwon (Hallym University) for providing the constructs used in this study and Dr. Seok Won Yim (Nesher Technologies) for providing technical support for ALEX fluorescence spectroscopy. We also thank Dr. Laurel Fisher (House Research Institute) for statistical analysis and Yoo Jin Lee (House Research Institute) for technical assistance.

Disclosures

The authors have no financial conflicts of interest.

References

- Lim, D. J. 1986. Functional structure of the organ of Corti: a review. *Hear. Res.* 22: 117–146.
- Lim, D. J. 1971. Vestibular sensory organs. A scanning electron microscopic investigation. *Arch. Otolaryngol.* 94: 69–76.
- Juhn, S. K. 1988. Barrier systems in the inner ear. *Acta Otolaryngol. Suppl.* 458: 79–83.
- Harris, J. P., and A. F. Ryan. 1995. Fundamental immune mechanisms of the brain and inner ear. *Otolaryngol. Head Neck Surg.* 112: 639–653.
- Okano, T., T. Nakagawa, T. Kita, S. Kada, M. Yoshimoto, T. Nakahata, and J. Ito. 2008. Bone marrow-derived cells expressing Iba1 are constitutively present as resident tissue macrophages in the mouse cochlea. *J. Neurosci. Res.* 86: 1758–1767.
- Hashimoto, S., P. Billings, J. P. Harris, G. S. Firestein, and E. M. Keithley. 2005. Innate immunity contributes to cochlear adaptive immune responses. *Audiol. Neurotol.* 10: 35–43.
- Adams, J. C., B. Seed, N. Lu, A. Landry, and R. J. Xavier. 2009. Selective activation of nuclear factor kappa B in the cochlea by sensory and inflammatory stress. *Neuroscience* 160: 530–539.
- Lecain, E., E. Sauvaget, P. Crisanti, T. Van Den Abbeele, and P. T. Huy. 1999. Potassium channel ether à go-go mRNA expression in the spiral ligament of the rat. *Hear. Res.* 133: 133–138.
- Lautermann, J., W. J. ten Cate, P. Altenhoff, R. Grümmer, O. Traub, H. Frank, K. Jahnke, and E. Winterhager. 1998. Expression of the gap-junction connexins 26 and 30 in the rat cochlea. *Cell Tissue Res.* 294: 415–420.
- Crouch, J. J., N. Sakaguchi, C. Lytle, and B. A. Schulte. 1997. Immunohistochemical localization of the Na-K-Cl co-transporter (NKCC1) in the gerbil inner ear. *J. Histochem. Cytochem.* 45: 773–778.
- Qu, C., F. Liang, W. Hu, Z. Shen, S. S. Spicer, and B. A. Schulte. 2006. Expression of CLC-K chloride channels in the rat cochlea. *Hear. Res.* 213: 79–87.
- Spicer, S. S., and B. A. Schulte. 1991. Differentiation of inner ear fibrocytes according to their ion transport related activity. *Hear. Res.* 56: 53–64.
- Yoshida, K., I. Ichimiya, M. Suzuki, and G. Mogi. 1999. Effect of proinflammatory cytokines on cultured spiral ligament fibrocytes. *Hear. Res.* 137: 155–159.
- Moon, S. K., R. Park, H. Y. Lee, G. J. Nam, K. Cha, A. Andalibi, and D. J. Lim. 2006. Spiral ligament fibrocytes release chemokines in response to otitis media pathogens. *Acta Otolaryngol.* 126: 564–569.
- Bernius, M., and D. Perlin. 2006. Pediatric ear, nose, and throat emergencies. *Pediatr. Clin. North Am.* 53: 195–214.
- Paparella, M. M., M. V. Goycoolea, and W. L. Meyerhoff. 1980. Inner ear pathology and otitis media. A review. *Ann. Otol. Rhinol. Laryngol. Suppl.* 89: 249–253.
- Paparella, M. M., T. Morizono, C. T. Le, F. Mancini, P. Sipilä, Y. B. Choo, G. Lidén, and C. S. Kim. 1984. Sensorineural hearing loss in otitis media. *Ann. Otol. Rhinol. Laryngol.* 93: 623–629.
- Casselbrant, M. L., J. M. Furman, E. Rubenstein, and E. M. Mandel. 1995. Effect of otitis media on the vestibular system in children. *Ann. Otol. Rhinol. Laryngol.* 104: 620–624.
- Bess, F. H., J. Dodd-Murphy, and R. A. Parker. 1998. Children with minimal sensorineural hearing loss: prevalence, educational performance, and functional status. *Ear Hear.* 19: 339–354.
- Casselbrant, M. L., R. J. Villardo, and E. M. Mandel. 2008. Balance and otitis media with effusion. *Int. J. Audiol.* 47: 584–589.
- Hunter, L. L., R. H. Margolis, J. R. Rykken, C. T. Le, K. A. Daly, and G. S. Giebink. 1996. High frequency hearing loss associated with otitis media. *Ear Hear.* 17: 1–11.
- Mutlu, C., A. O. Odabasi, K. Metin, S. Basak, and G. Erpek. 1998. Sensorineural hearing loss associated with otitis media with effusion in children. *Int. J. Pediatr. Otorhinolaryngol.* 46: 179–184.
- Kawauchi, H., T. F. DeMaria, and D. J. Lim. 1989. Endotoxin permeability through the round window. *Acta Otolaryngol. Suppl.* 457: 100–115.
- Cook, R. D., D. S. Postma, G. M. Brinson, J. Prazma, and H. C. Pillsbury. 1999. Cytotoxic changes in hair cells secondary to pneumococcal middle-ear infection. *J. Otolaryngol.* 28: 325–331.
- Ichimiya, I., M. Suzuki, T. Hirano, and G. Mogi. 1999. The influence of pneumococcal otitis media on the cochlear lateral wall. *Hear. Res.* 131: 128–134.
- Tsuprun, V., S. Cureoglu, P. A. Schachern, P. Ferrieri, D. E. Biles, M. M. Paparella, and S. K. Juhn. 2008. Role of pneumococcal proteins in sensorineural hearing loss due to otitis media. *Otol. Neurotol.* 29: 1056–1060.
- Moon, S. K., J. I. Woo, H. Y. Lee, R. Park, J. Shimada, H. Pan, R. Gellibolian, and D. J. Lim. 2007. Toll-like receptor 2-dependent NF-kappaB activation is involved in nontypeable *Haemophilus influenzae*-induced monocyte chemotactic protein 1 up-regulation in the spiral ligament fibrocytes of the inner ear. *Infect. Immun.* 75: 3361–3372.
- Woo, J. I., H. Pan, S. Oh, D. J. Lim, and S. K. Moon. 2010. Spiral ligament fibrocyte-derived MCP-1/CCL2 contributes to inner ear inflammation secondary to nontypeable *H. influenzae*-induced otitis media. *BMC Infect. Dis.* 10: 314.
- Feng, L., Y. Xia, T. Yoshimura, and C. B. Wilson. 1995. Modulation of neutrophil influx in glomerulonephritis in the rat with anti-macrophage inflammatory protein-2 (MIP-2) antibody. *J. Clin. Invest.* 95: 1009–1017.
- Schrier, D. J., R. C. Schimmer, C. M. Flory, D. K. Tung, and P. A. Ward. 1998. Role of chemokines and cytokines in a reactivation model of arthritis in rats induced by injection with streptococcal cell walls. *J. Leukoc. Biol.* 63: 359–363.
- Skidgel, R. A., X. P. Gao, V. Brovkovich, A. Rahman, D. Jho, S. Predescu, T. J. Standiford, and A. B. Malik. 2002. Nitric oxide stimulates macrophage inflammatory protein-2 expression in sepsis. *J. Immunol.* 169: 2093–2101.
- Kim, D. S., J. H. Han, and H. J. Kwon. 2003. NF-kappaB and c-Jun-dependent regulation of macrophage inflammatory protein-2 gene expression in response to lipopolysaccharide in RAW 264.7 cells. *Mol. Immunol.* 40: 633–643.
- Sohn, W. J., K. W. Lee, Y. Lee, J. H. Han, Y. K. Choe, D. S. Kim, and H. J. Kwon. 2005. Pyrrolidine dithiocarbamate-induced macrophage inflammatory protein-2 gene expression is NF-kappaB-independent but c-Jun-dependent in macrophage cell line RAW 264.7. *Mol. Immunol.* 42: 1165–1175.
- Lee, K. W., Y. Lee, H. J. Kwon, and D. S. Kim. 2005. Sp1-associated activation of macrophage inflammatory protein-2 promoter by CpG-oligodeoxynucleotide and lipopolysaccharide. *Cell. Mol. Life Sci.* 62: 188–198.
- Barenkamp, S. J., and E. Leininger. 1992. Cloning, expression, and DNA sequence analysis of genes encoding nontypeable *Haemophilus influenzae* high-molecular-weight surface-exposed proteins related to filamentous hemagglutinin of *Bordetella pertussis*. *Infect. Immun.* 60: 1302–1313.
- Moon, S. K., H. Y. Lee, H. Pan, T. Takeshita, R. Park, K. Cha, A. Andalibi, and D. J. Lim. 2006. Synergistic effect of interleukin 1 alpha on nontypeable *Haemophilus influenzae*-induced up-regulation of human beta-defensin 2 in middle ear epithelial cells. *BMC Infect. Dis.* 6: 12.

87. Mkaddem, S. B., C. Werts, J. M. Goujon, M. Bens, E. Pedruzzi, E. Ogier-Denis, and A. Vandewalle. 2009. Heat shock protein gp96 interacts with protein phosphatase 5 and controls toll-like receptor 2 (TLR2)-mediated activation of extracellular signal-regulated kinase (ERK) 1/2 in post-hypoxic kidney cells. *J. Biol. Chem.* 284: 12541–12549.
88. Chen, L., M. G. Oakley, J. N. Glover, J. Jain, P. B. Dervan, P. G. Hogan, A. Rao, and G. L. Verdine. 1995. Only one of the two DNA-bound orientations of AP-1 found in solution cooperates with NFATp. *Curr. Biol.* 5: 882–889.
89. Ryseck, R. P., and R. Bravo. 1991. c-JUN, JUN B, and JUN D differ in their binding affinities to AP-1 and CRE consensus sequences: effect of FOS proteins. *Oncogene* 6: 533–542.
90. Kerppola, T. K., and T. Curran. 1994. A conserved region adjacent to the basic domain is required for recognition of an extended DNA binding site by Maf/Nrl family proteins. *Oncogene* 9: 3149–3158.
91. Rajaram, N., and T. K. Kerppola. 1997. DNA bending by Fos-Jun and the orientation of heterodimer binding depend on the sequence of the AP-1 site. *EMBO J.* 16: 2917–2925.